WRF Simulations to Investigate Processes Across Scales (WRFSCALE)

Hans-Stefan Bauer, Thomas Schwitalla, Oliver Branch, Rohith Thundathil, Stephan Adam, and Volker Wulfmeyer

Abstract Several scientific aspects ranging from boundary layer research and land modification experiments to data assimilation applications were addressed with the Weather Research and Forecasting (WRF) model from the km-scale down to the turbulence-permitting scale. Case study simulations in as different regions as the central United States, the United Arab Emirates and southwestern Germany were performed to investigate the evolution of the convective boundary layer. The multi-nested WRF setup, driven by the operational analysis of the European Centre for Medium-range Weather Forecasts (ECMWF), high-resolution terrain, and land cover data sets simulated a realistic evolution of the internal turbulent structure of the boundary layer including the transitions between daytime and nighttime conditions. Land modification simulations in the United Arab Emirates demonstrated that plantations as small as $10 \times 10\,\mathrm{km}^2$ could modify the weather pattern in this area in a way that more precipitation reaches the desert. Data assimilation experiments demonstrated the beneficial influence of state-of-the-art lidar measurements on the forecast performance of WRF. A further improvement was found when the more sophisticated hybrid 3DVAR-ETKF method was applied, since this method includes a flow-dependent model error contribution and thus more realistically spreading the information of the observations.

H.-S. Bauer (✉) · T. Schwitalla · O. Branch · R. Thundathil · S. Adam · V. Wulfmeyer
Institute of Physics and Meteorology, Garbenstrasse 30, 70599 Stuttgart, Germany
e-mail: hans-stefan.bauer@uni-hohenheim.de

T. Schwitalla
e-mail: thomas.schwitalla@uni-hohenheim.de

O. Branch
e-mail: oliver_branch@uni-hohenheim.de

R. Thundathil
e-mail: rohith.thundathil@uni-hohenheim.de

S. Adam
e-mail: stephan_adam@uni-hohenheim.de

V. Wulfmeyer
e-mail: volker.wulfmeyer@uni-hohenheim.de

W. E. Nagel et al. (eds.), *High Performance Computing in Science and Engineering '19*,
https://doi.org/10.1007/978-3-030-66792-4_34

1 Introduction and Motivation

Numerical models have the potential to address the inherent weaknesses of observation-based approaches, since they can provide a full 4D representation of the atmosphere and produce a consistent state with respect to the 3D thermodynamic atmospheric fields, cloud water, cloud ice, and diagnostic variables such as precipitation. Therefore, numerical models are excellent tools to improve our understanding of atmospheric processes across scales.

Recent results have demonstrated that grid resolutions of less than around 4 km are necessary for a realistic representation of mesoscale processes, especially in terms of the spatial and temporal distribution of precipitation. Further improvements are expected if a chain of grid refinements is performed down to the Large-Eddy Simulation (LES) scale (100 m and below), as further details of land-surface atmosphere (LSA) interaction are resolved. Through application of extremely high resolution and low-pass filtering, larger eddies and the dominant spectra for turbulent transport of heat and moisture can be simulated explicitly.

The WRF model system, described with more detail in earlier reports, provides the opportunity to perform LES simulations under realistic conditions because of the wide range of scales it can be applied over. Using a nesting strategy that covers the synoptic weather situation and the mesoscale circulations, in combination with data assimilation, will ensure a forcing of the LES that is as close as possible to the real weather situation.

2 Work Done Since July 2018

2.1 LES Simulations to Better Understand Boundary Layer Evolution and High-Impact Weather (LES-PROC)

The four-dimensional results of high-resolution numerical weather prediction models provide excellent data sets for detailed investigations of the evolution of the boundary layer.

In August 2017, the **L**and **A**tmosphere **F**eedback **E**xperiment (LAFE) took place at the Southern Great Plains site of the Atmospheric Radiation Measurement Program (ARM) in Oklahoma. Many different instruments were brought to the site and the measurement strategy was optimized in a way to derive as much information as possible. The goals of the campaign were:

1. Determine turbulence profiles and investigate new relationships among gradients, variances, and fluxes.
2. Map surface momentum, sensible heat, and latent heat fluxes using a synergy of scanning wind, humidity, and temperature lidar systems.
3. Characterize land-atmosphere feedback and the moisture budget.

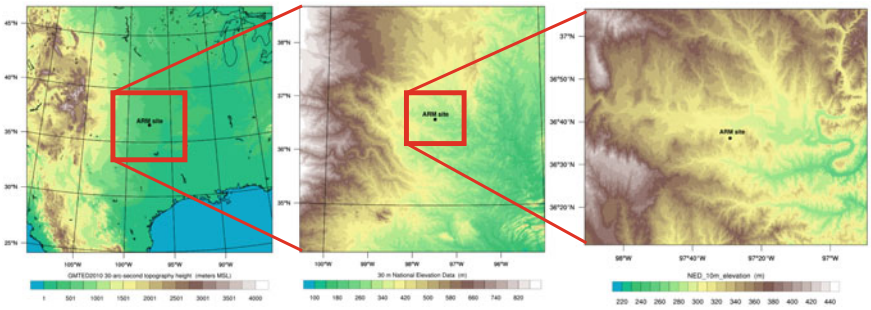

Fig. 1 Domain configuration of the first LAFE simulation. From left to right the domains with 2500 m, 500 m and 100 m are shown

4. Verify large-eddy simulation model runs and improve turbulence representations in mesoscale models.

More details about the campaign and the applied measurement strategy can be found in [4].

Within LES-PROC simulations of selected case studies during the campaign will be carried out to perform detailed comparisons with observations, contributing to goal four of LAFE. A first simulation down to turbulence-permitting resolution of 100 m was carried out for the 23rd of August 2017, one of the golden measurement days during the campaign. It was a clear sky day where the operation of the lidar systems was temporally extended to include the evening transition of the convective boundary layer.

The simulation was started at 06 UTC (01 local time) and run for more than 22 h within the 24 h walltime limit. With this, it was our first simulation containing both the morning and the evening transitions between the nighttime stable and the daytime convective boundary layer. WRF was set-up in a three-domain configuration with 2500 m, 500 m and 100 m resolution and the outer domain was driven by the operational analysis of the European Centre of Medium Range Weather Forecasting (ECMWF). The size of the domains is 1000×1000, 1001×1001 and 1201×1001 grid cells with 100 vertical levels in each domain. Figure 1 illustrates the domain setup. The location of the ARM site is marked in the different domains.

Figure 2 shows the development of the 10 m horizontal wind field for two time steps in the morning and the afternoon local time. In the morning local time (left panel), the turbulence is still weak, resulting in typical role-like circulation patterns. Later in the afternoon (right panel), with fully developed turbulence, the roles break apart into turbulent eddies, leading to the development of small-scale gust fronts. Interestingly, coherent structures caused by the underlying orography are seen, demonstrating the benefits of simulations with such high horizontal resolution.

Figure 3 illustrates the fully developed convective boundary layer 1000 m above sea level in the afternoon of August 23. The vertical velocity field 1000 m above sea level illustrates a typical convective boundary layer undisturbed by clouds. The cir-

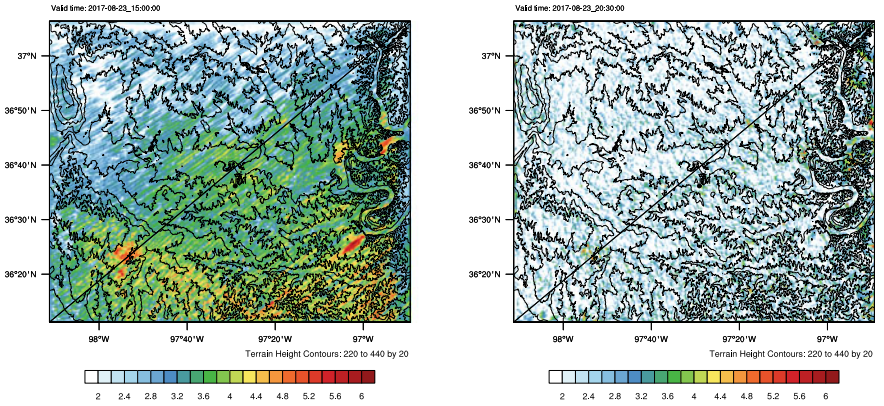

Fig. 2 10 m horizontal wind velocity $[ms^{-1}]$ for 10 a.m. (left) and 3:30 p.m. (right). Shown is the innermost domain with 100 m horizontal resolution

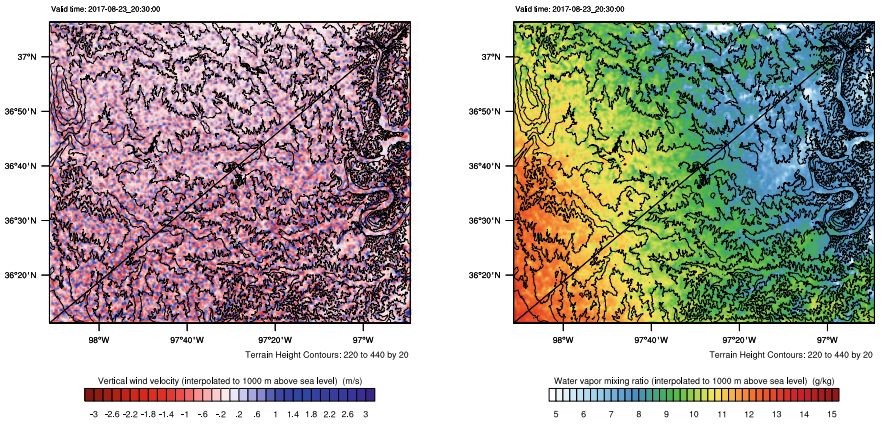

Fig. 3 Vertical wind velocity $[ms^{-1}]$ (left) and water vapor mixing ratio $[gkg^{-1}]$ (right) 1000 m above sea level in the well-developed boundary layer at 3:30 p.m., 23 August 2017 as simulated by WRF with 100 m horizontal resolution

culation broke apart into turbulent eddies of different size. Small regions of intense updrafts (blue) are surrounded by larger regions of weaker compensating downdrafts (red). The sizes of the developing structures correspond to observations. Furthermore, regions over flat terrain where the turbulence develops isotropically can be separated from regions where coherent structures develop influenced by the underlying orography.

The updraft regions can also be identified in the water vapor field (right panel) as moist bubbles. Furthermore, a large-scale southwest-to-northeast gradient in moisture with larger values in the elevated western and especially southwestern parts of the domain is seen. The large-scale meteorological forcing provided by the ECMWF analysis via the two coarser domains is the main cause for the observed behavior.

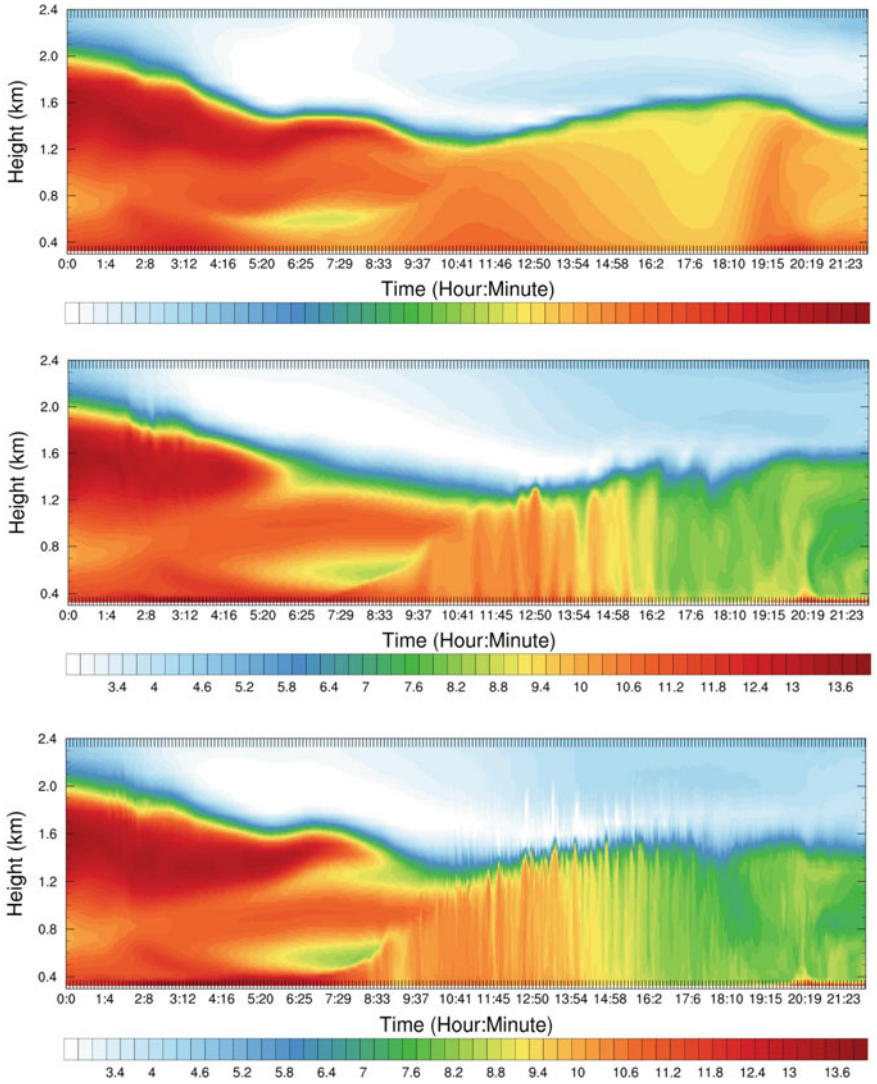

Fig. 4 Time-height cross section of the water vapor mixing ratio $[gkg^{-1}]$ for the grid cell the Hohenheim lidar systems were located over the full forecast range. From top to bottom: 2500 m, 500 m and 100 m horizontal resolution

Figure 4 shows time-height cross sections of water vapor mixing ratio for the grid cell the Hohenheim lidar systems were located for the three different horizontal resolutions of the model chain.

The coarsest resolution, applying a turbulence parameterization, shown in the top panel, is only capable to reproduce the correct height of the boundary layer. The expected internal structure of the boundary layer and the undulating top of the

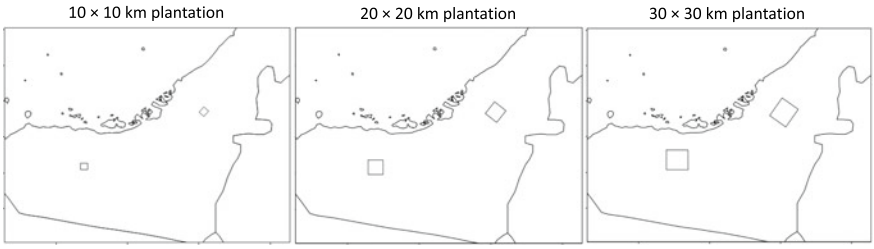

Fig. 5 Three plantation scenarios of different sizes showing square plantations of dimensions 10 km, 20 km and 30 km placed in the desert of the UAE

boundary layer cannot be simulated with a turbulence parameterization. Furthermore, spurious wave-like structures are simulated in the moisture field. In the simulation with 500 m resolution and switched-off turbulence parameterization, internal structure starts to develop, but the resolution is too coarse to capture the expected fine-scale turbulent eddies. The simulation with the highest 100 m resolution nicely captures the morning and evening transitions and the internal structure of the boundary layer.

2.2 Seasonal Land Surface Modification Simulations over the United Arab Emirates (UAE-1)

Previous studies have demonstrated that large-scale land surface modifications can affect the weather, and potentially in a controllable and predictable way [1–3]. However, these studies have all been based on very large scales of $100 \times 100\,km^2$. Furthermore, these simulations were in other regions and it is not known if similar impacts could occur in the UAE region.

The goal of sub-project UAE-1 is to assess the impact of smaller and more feasible land surface modification scenarios. This was done via single day simulations with the WRF-NOAHMP model under varying atmospheric conditions. Figure 5 shows three selected scenarios with three different sizes of plantation—10 km, 20 km and 30 km (square). These simulations were compared with control runs without plantations.

Figure 6 shows phenomena occurring in one of the case studies (27 July 2015). The left panel shows the change in net surface radiation at the surface caused by the reduced albedo of the plant canopy. This leads to a rise in 2m temperatures (vector colors) and a low pressure disturbance. This leads to a wind convergence and corresponding ascent of air. The right panel shows an increase in turbulence over the plantation caused by both heating and increased surface roughness.

With ascending air and increased turbulent transport, the level of free convection can be reached upon which a convective cell develops. Figure 7 shows the respective impacts on rainfall over the whole day from all three scenarios. It is clear that all sizes have a large impact on rainfall (In the control, not shown, there is little rainfall

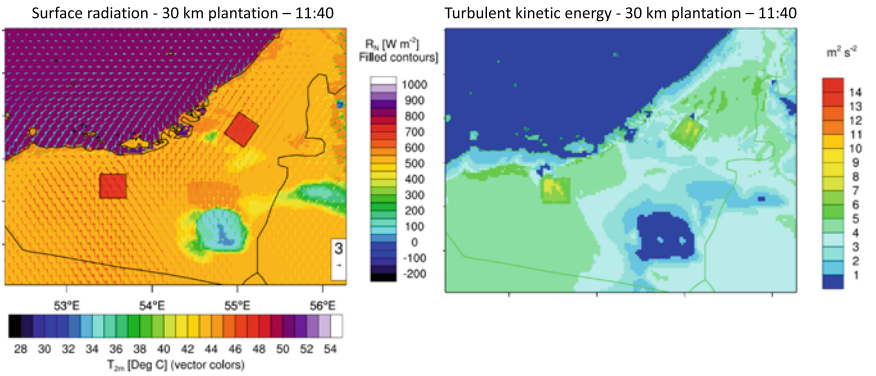

Fig. 6 Instantaneous impact on surface radiation, windflow and 2m temperatures (left) and on turbulent kinetic energy (right)

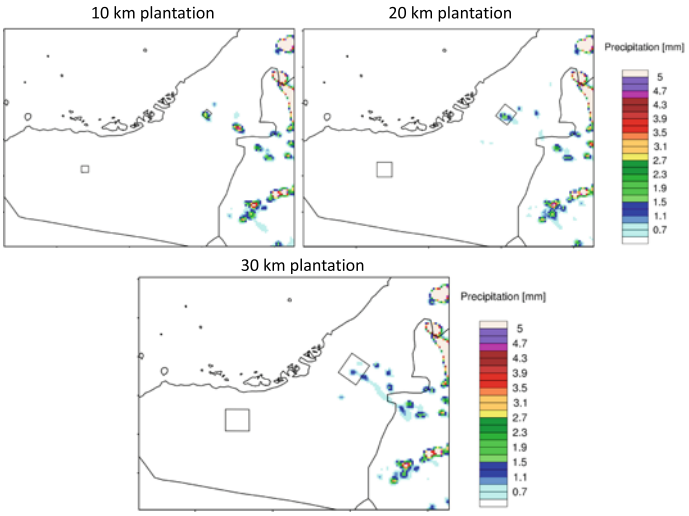

Fig. 7 Accumulated rainfall on 27 July 2015 for all three scenarios [mm] ending at 00:00 UTC

around the plantation areas). However, there is a difference in impact from the scale of the plantations both spatially and in the amounts.

Figure 8 shows the integrated rainfall amounts in a 50 km radius around the plantation areas in m^3. This larger integration zone was chosen because some rainfall occurs outside the plantation boundaries. We can see that all scenarios exhibit an increase in precipitation compared to the control and also that the amounts scale with size. However, the scaling is not that significant and a key finding is that plantations as small as 10 km have a very large impact. If we assume there are at least five cases during a summer period we could expect water amounts of at least 1,000,000

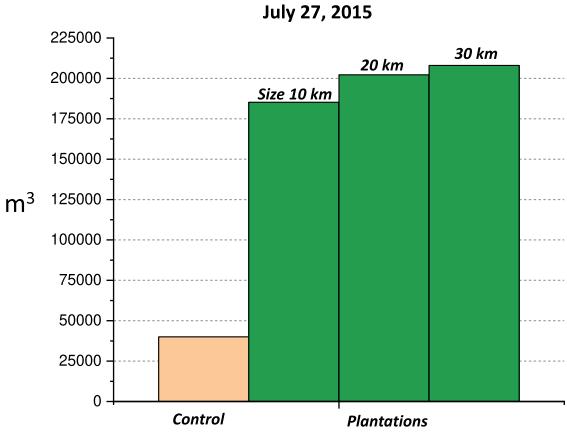

Fig. 8 Integrated rainfall amounts reaching the ground from each scenario [m^3]

m^3. Taking into account the amount of irrigation water required for Jojoba this would be enough to offset 3 km^2 of plantation area.

In summary, these simulations indicate that conditions in summer in the UAE are conducive for impacts from small plantations down to 10 km size. It is also clear from rainfall amounts that there is a dependency on plantation size but it is not as significant as one might have estimated.

These findings have profound implications for all arid regions and in particular the UAE, which suffers greatly from water scarcity. Furthermore, there are exciting implications for using plantations as a weather modification method, a field of study, which until now, has focused primarily on cloud seeding. If the weather modification is predictable, it can form a synergy with the potential of plantations for significant carbon storage.

2.3 Data Assimilation and Forecasting Over the United Arab Emirates (UAE-2)

The initial set up with a nesting ratio of 1:5 ending at 111 m grid increment led to difficulties in simulating the cloud development over the Al Hajar Mountains because the steep gradient leads to an unstable behavior. The WRF model is based on a terrain following coordinate system and a true horizontal diffusion scheme is applied. According to the WRF developers, this pushes the applied numeric to its limits as the slope at this particular resolution exceeds 40^o. A suggestion by the WRF developers is to heavily smooth terrain but this is not our intention on the turbulence permitting scale.

Therefore, it was necessary to revise our setup and we then applied a nesting ratio of 1:3 so that currently the finest grid increment is 309 m with an intermediate nest of 926 m grid increment. We also tested a fourth domain with 103 m grid increment

Table 1 Model domain configuration and resolutions

Domain	Grid Cells	Vertical levels	Grid increment	Time step (s)	Domain size
D01	900 ∗ 700	100	0.025^o (2.8 km)	10	2500 km × 2500 km
D02	790 ∗ 790	100	0.0083^o (926 m)	3	732 km × 732 km
D03	826 ∗ 772	100	0.0027^o (309 m)	1	255 km × 239 km

but we could not generate results due to numerical instability. Table 1 summarizes the grid dimensions and resolutions.

Domains D01 and D02 were run concurrently in a one-way-nested approach while D03 was forced by the 5 min output of D02 using the NDOWN approach. The NDOWN approach allows for running a domain not directly coupled to the outer domains. It makes use of high-frequency temporal output files of the parent domains available in few minute intervals. For D03, two simulations with and without a PBL scheme were conducted.

The upper row of Fig. 9 shows an example for the different results with and without a PBL parametrization of the 2 m temperatures together with the 10 m wind field at 309 m resolution. The lower row of Fig. 9 shows the simulated cloud liquid water path. From the upper row, it is clearly visible that a simulation without PBL parametrization simulates higher 2 m temperature with a difference of almost 4 K. Both simulations show similar cloud patterns, although it appears that the simulation with an applied PBL parameterization simulates less strong convection, which is partly reflected in the rainfall patterns (not shown here). The maximum rainfall amount is approx. 13 mm in case no PBL scheme is applied and 24 mm when a PBL scheme is applied. Apparently, the PBL scheme supports the development of convection in this particular case.

Figure 10 shows every minute model time series of vertical velocity at one grid point west of Al Ain where daytime turbulence is nicely visible as indicated by the changing colors.

The turbulence permitting simulation was conducted for 18 h forecast time and is initialized six hours after D01 and D02 at 06 UTC on 14 July, 2015. The computation required 7200 compute cores on the Cray XC40 system for about 12 h wall clock time resulting in an output data volume of 7.2 TB assuming 1 min output only in D03 for process studies.

In addition to the turbulence permitting simulation, we decided to set up a five-member physics ensemble with different combinations of PBL and cloud microphysics in order to achieve a sufficient spread among the simulations at the convection permitting resolution of 2.7 km.

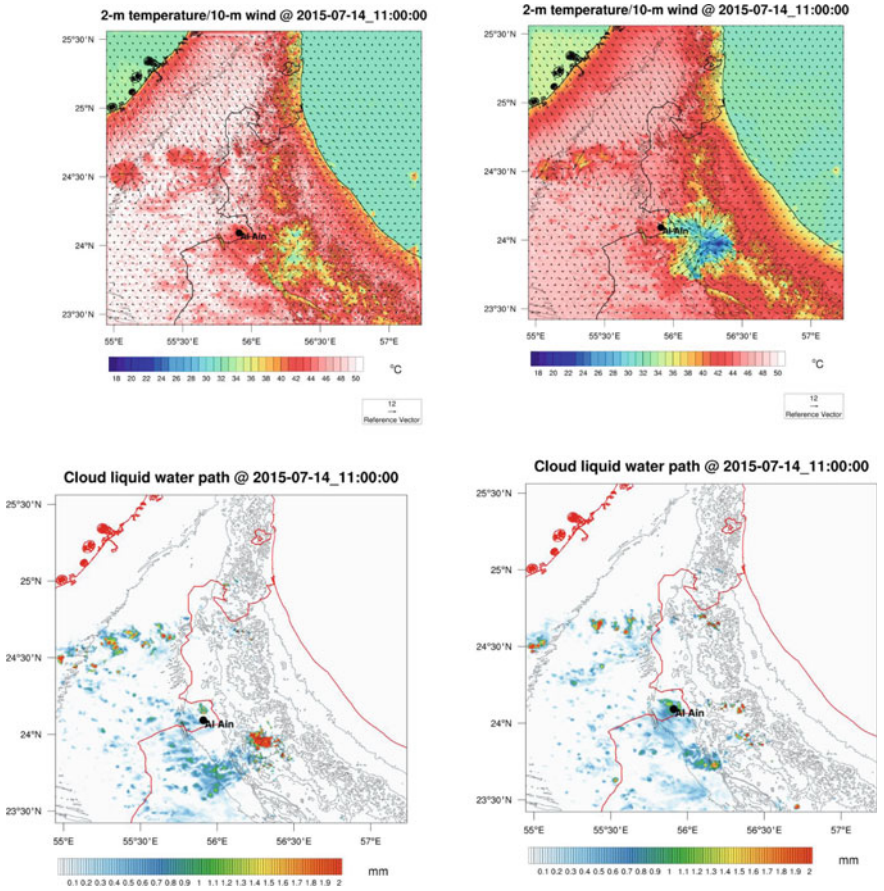

Fig. 9 Upper row: 2-m temperatures [^oC] of the turbulence-permitting domain with PBL (left) and without a PBL parametrization. Lower row: Same as the upper row but for the cloud water path [mm]

Downscaling simulations for the 14 July 2015 case study without data assimilation were performed and are currently being analyzed. The output data volume of the whole ensemble is around 7 TB with 15 min output frequency.

With the available station observations from the National Center for Meteorology (NCM) in Abu Dhabi, we validated the diurnal cycle of 2 m temperature, 2 m dew point as well as 10 m wind speeds. Figure 11 shows an example of the diurnal cycles of the 2-m temperature over the UAE for the different configurations compared to the NCM station observations.

All WRF configurations show a negative temperature bias before sunrise and after sunset. As the 2-m dewpoint and 10-m wind speeds do not show a significant deviation, it is assumed that the model has difficulties in predicting the strong nocturnal inversion layer. This is a well-known problem for almost all mesoscale models.

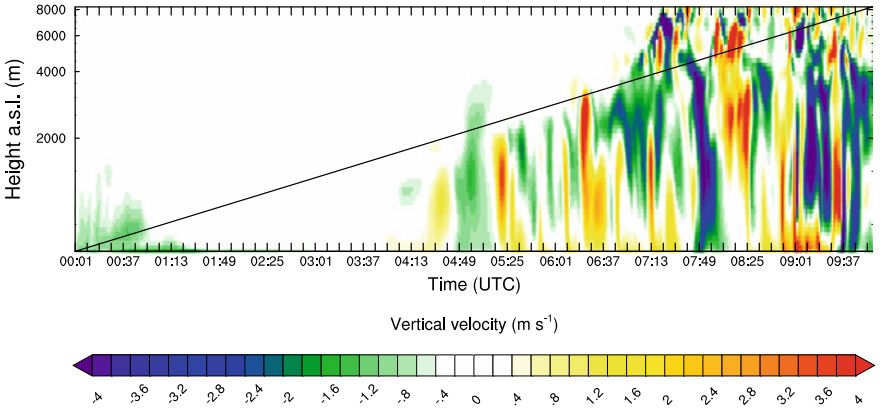

Fig. 10 Time series of the simulated vertical velocities west of Al Ain. The temporal resolution is 60 s

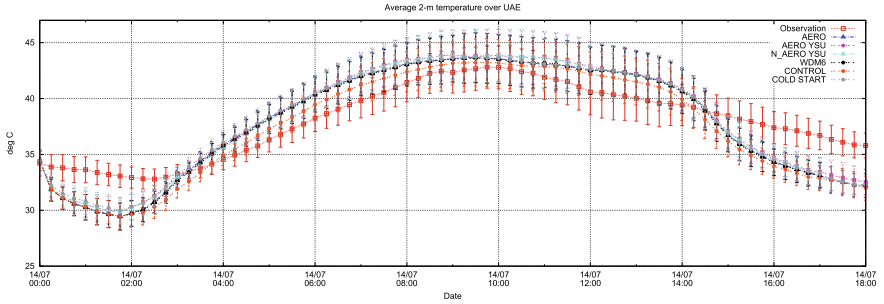

Fig. 11 Mean diurnal cycle of the 2-m temperatures over the UAE on July 14th, 2015

However, further details are very difficult to examine, as no vertical profiling data of temperature are available yet.

Regardless of these deviations, our initial results demonstrate a most realistic representation of the cloud pattern by the combination of the YSU PBL and Thompson Aerosol-aware cloud microphysics, when compared to the cloud liquid water (LWP) path obtained from the Climate Monitoring Satellite Application Facility (CMSAF) based on the SEVIRI imaginary from MSG-2. The product has a spatial resolution of 0.05° and is currently available every 15 min during daytime until the end of 2015.

Figure 12 shows an example of the observed and simulated LWP at 14 July 2015 12 UTC. It is seen that the simulation shows more dense water clouds in case the YSU PBL is applied (right panel). Compared to the simulations with the Thompson cloud microphysics schemes, the configuration with the WDM6 microphysics scheme (middle panel) simulates considerably less water clouds but instead produces too many ice clouds which does not happen to the other configurations.

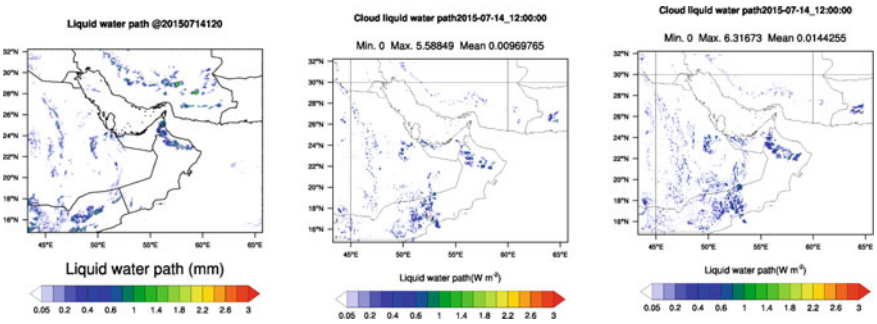

Fig. 12 Observed cloud liquid water (CWP) path [mm] from MSG SEVIRI (left). Simulated CWP applying different combinations of PBL and cloud microphysics schemes

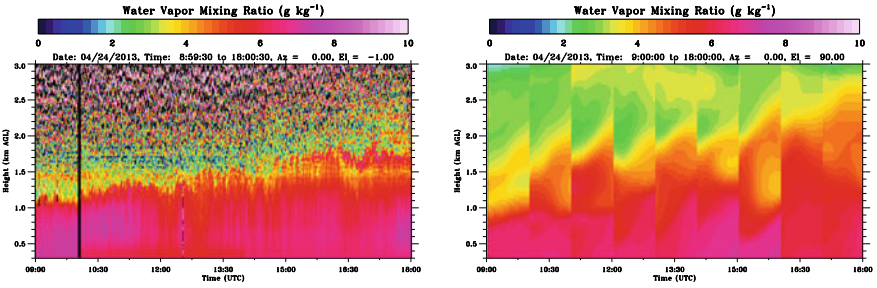

Fig. 13 Left panel: 1-min Water vapor mixing ratio from the DIAL from 09 UTC to 18 UTC. Right panel: 1-min Water vapor mixing ratio model output after assimilation with 3DVAR RUC DA in the same time period

2.4 Assimilation of Lidar Water Vapor Measurements (VAP-DA)

Water vapor plays a crucial role in the atmosphere although its fraction is comparatively less among the other constituents. Humidity content in the atmosphere has its effect on the overall dynamics, radiation and significantly in the development of clouds and precipitation as well. With the advent of lidar systems, promising research on the interaction of water vapor on various scales of the atmosphere had its commencement. With its robust and fast measurements with high temporal and spatial resolution, a huge amount of high-quality data can be measured. These measurements are crucial for process understanding in the atmosphere and especially in the boundary layer where rapid changes result in significant influence on the future state.

Assimilation of the high quality data obtained from lidar instruments is a good leap in numerical weather prediction. For NWP models, a better initial state determines the quality of the forecast. A lidar data network has a huge potential to close the voids in the data availability present in the lower troposphere where the only

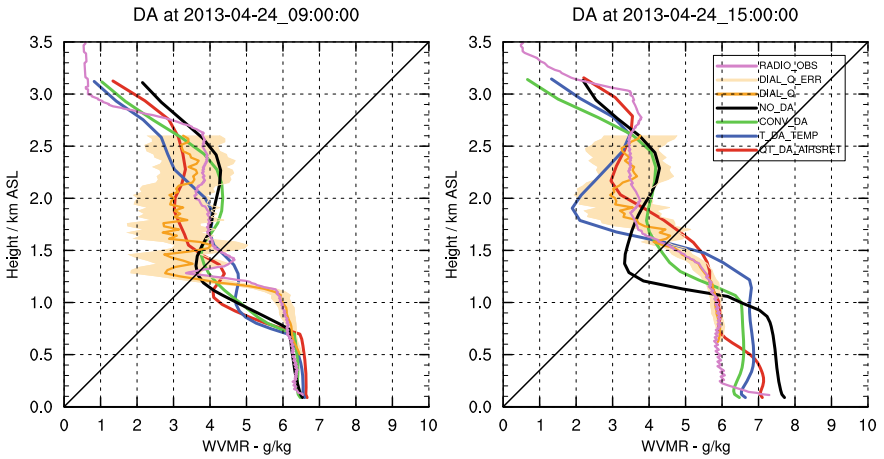

Fig. 14 Left panel: Water vapor mixing ratio $[g/kg]$ profile during the first assimilation. Right panel: Water vapor mixing ratio profile at 15 UTC after 6 assimilation cycles

quality data is provided by radiosondes, which still has shortcomings. Instantaneous measurements like radiosondes cannot capture the changes in the atmosphere that can be registered by continuous measurements by the lidars. Assimilation of water vapor lidar measurements into the NWP model WRF was a limitation in the past few years since there hadn't been a suitable forward operator for the direct assimilation of water vapor mixing ratio which is one of the major prognostic variables in the WRF model. Within WRFSCALE, a forward operator for the direct assimilation of water vapor mixing ratio profiles has been accomplished with the modification of the atmospheric infrared sounding retrieval (AIRSRET) operator already available in the WRFDA system.

The assimilation of water vapor profiles into the model was successful and resulted in a positive impact. The assimilation was performed with the three-dimensional variational (3DVAR) data assimilation approach initially and now being tested for ensemble data assimilation methods. The test case for the DA technique was the data obtained from one intensive observation period (IOP) of the HOPE campaign which was held in western Germany during the month of April and May 2013. A 10-hour dataset was assimilated into the model with hourly data inputs. A rapid update cycle 3DVAR data assimilation was performed at hourly intervals for the entire European domain at a spatial resolution of 2.5 km and a vertical resolution of 100 levels up to 50 hPa. More vertical levels were defined below two km of height where assimilation of more data points are required due to the strong variability of the mixing ratio in the boundary layer.

The assimilation of the water vapor mixing ratio profiles corrects the model at hourly intervals where the DIAL data is fed into the model. Figure 13 shows a direct comparison of the time series output from the model with the observed water vapor mixing ratio (WVMR) from the DIAL. The profile plot in Fig. 14 shows the impact

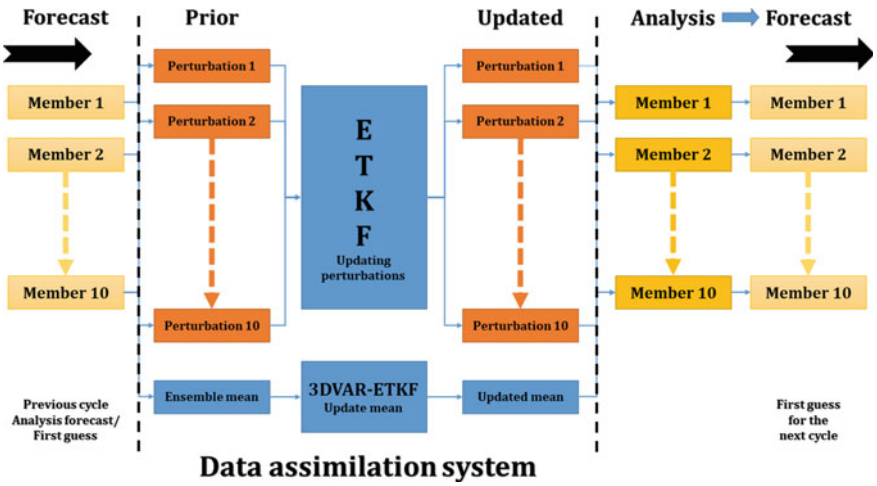

Fig. 15 Schematic of the hybrid 3DVAR-ETKF data assimilation system with 10 ensemble members

of assimilation on the vertical profile at the first assimilation and after six assimilation cycles. The 15 UTC assimilation shows good agreement with the DIAL profile although the model couldnt capture the boundary layer gradient in the first assimilation at 9 UTC.

Another data assimilation technique to incorporate flow-dependent forecast error covariances into the assimilation process is currently being tested for the same domain to alleviate the effects of the static covariance of the 3DVAR assimilation system. The ensemble technique implemented for this purpose is the hybrid 3DVAR-ensemble transform Kalman filter (ETKF) where the error covariance matrix in the assimilation system is a combination of static and flow-dependent covariances. Thus, the model has a lesser dependence on the static background error covariance matrix previously determined to minimize the cost function.

Figure 15 illustrates the data assimilation process undergone in the 3DVAR-ETKF data assimilation. The assimilation system starts with a set of currently 10 ensemble members each with the same configuration as the previous experiments with a spatial resolution of 2.5 km and vertical resolution of 100 levels. The mean of the set of ensemble members are derived along with the variance of the members as well. With the generated mean the perturbations of the individual ensemble members from the mean are calculated. These perturbations are updated by the ETKF and the mean of the ensemble members is assimilated with the combination of the analysis covariance matrix obtained from the variance of the ensemble members and the previously determined static covariance matrix.

The hybrid output generated from the assimilation can be continued for next cycles. The updated perturbations from the ETKF is added to the ensemble mean to get the next set of ensemble members which now are the analysis ensemble members.

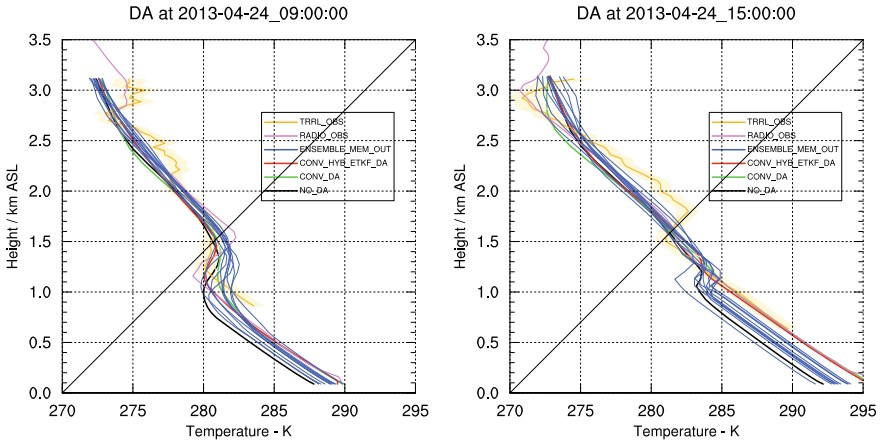

Fig. 16 Temperature profile plot for a conventional 3DVAR DA and conventional 3DVAR-ETKF DA. Left panel: Assimilation performed at 09 UTC. Right panel: Assimilation at 15 UTC after six assimilation cycles

These analysis ensemble members are forecasted along with the hybrid ensemble output to get the next first guess or the background ensemble members.

Figure 16 shows the impact of assimilation of conventional data on the temperature profiles. The hybrid 3DVAR-ETKF out which is shown in the red color has a slightly better agreement with observed data which is the radiosonde and the temperature Raman lidar (TRRL). The blue lines are the 10 ensemble member outputs, which are obtained after adding the mean to the ETKF perturbations in the data assimilation process.

2.5 LES for SABLE and the AMMER Catchment (LES-PBL)

Nested large eddy simulations (LES) with the weather research and forecast model (WRF) have been conducted. Operating LES with an NWP model has the advantage of simulating the turbulent exchange processes between the land surface and the atmosphere of the moisture, heat and momentum in the planetary boundary layer (PBL) under realistic conditions. Therefore, the impact of a specific weather situation on the development and the transport happening inside the PBL can be investigated. Simulations for two cases studies for the Ammer catchment west of Tuebingen have been made. One case was the 15th of July 2015 (AMMER2015), which was in a distinct dry period and the other the 09th of June 2016 (AMMER2016), which took place after a heavy precipitation event, with soil moistures close to saturation. Thus, the surface forcing differed for both cases, with much higher surface sensible heat flux S_h found for the 2015 case (250 W/m^2 in the domain mean) than for the 2016 case (200 W/m^2 in the domain mean). Furthermore, the 2015 case study was very

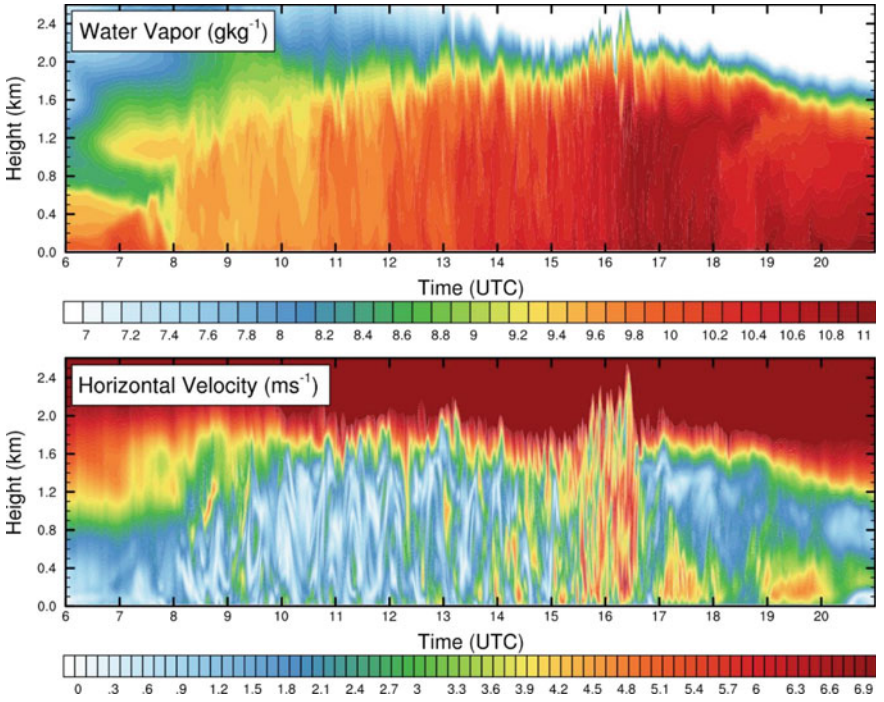

Fig. 17 Time-height cross section of the water vapor mixing ratio q_v $[g/kg]$ (top) and the horizontal wind velocity u_h $[m/s]$ (bottom) for the AMMER2015 case study. The temporal resolution is 10 s

calm with maximum mean horizontal wind velocities of 2 m/s compared to 9 m/s found for the 2016 case.

Figures 17 and 18 present time-height cross sections of the water vapor mixing ratio q_v and the horizontal wind velocity u_h for both the 2015 and the 2016 case study at the town of Entringen, located in the Ammer catchment. For the AMMER2015 case, an accumulation of moisture in the PBL (Fig. 17) is found. Relatively high values of around 2.0 km for the depth of the turbulent PBL (z_i) are found. The height of the PBL z_i is visible at the level with the largest decrease of q_v with height. The exchange of the air from the atmosphere above z_i and the PBL (entrainment) is limited to the upper part of the PBL. The horizontal wind velocity u_h in the PBL shows for most of the case relatively low values up to 2 m/s in the PBL.

For the AMMER2016 case, a decrease in the moisture inside the PBL during daytime is found (Fig. 18). The time-height cross section shows a growth of the PBL into an already relatively moist residual layer. Entrainment of dry air into the PBL can be identified as one factor for decreasing q_v in the PBL during daytime. After 1200 UTC, a series of dry tongues reaching down to the surface are visible in the moisture field of the PBL. Over the day, the horizontal wind velocity stays constant on relatively large values of around 7 m/s, with larger variations in the evening. Smaller

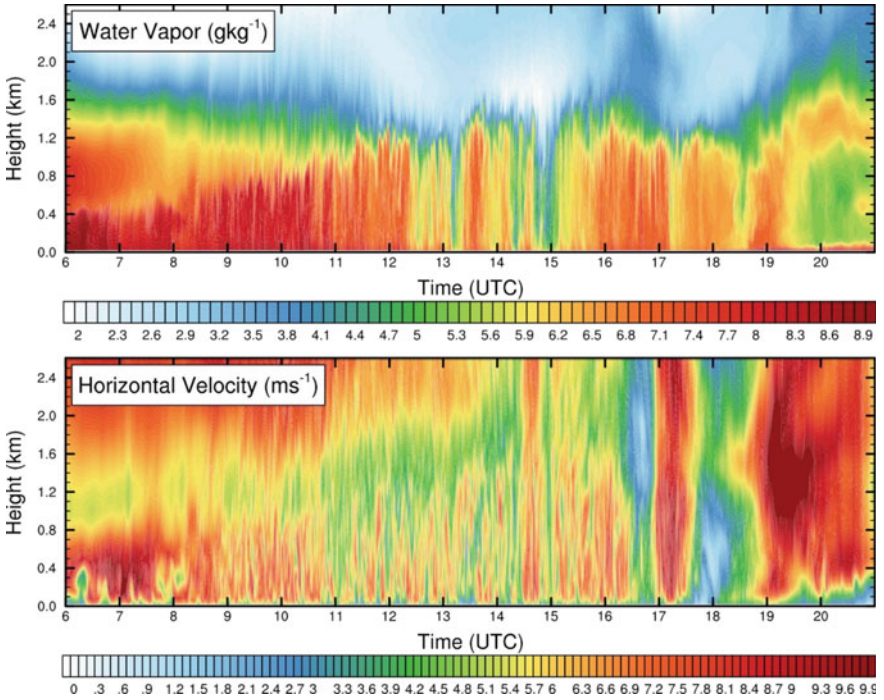

Fig. 18 Same as Fig. 17, but for the AMMER2016 case study

maximum values for z_i are found compared to the AMMER2015 case. This is in accordance with the smaller sensible heat fluxes found for the AMMER2016 case.

The differences in the horizontal wind velocity between the 2015 and the 2016 case have an influence on the organization of the convection in the PBL. Figure 19 presents the instantaneous values of the horizontal moisture flux convergence in the lower PBL for both cases.

Positive flux convergence is found in areas where updrafts are forming and negative values in areas with downdrafts. Due to the mass balance, the moist air in the lower PBL is converging in the area of updrafts, while in the area of downdrafts, dryer air from higher altitudes is transported downwards.

For the AMMER2015 case (Fig. 19a), a rather unstructured field of the moisture flux convergence is found. Clear signs for open cell convection are found, with relatively distinct areas where updrafts are forming, separated with larger areas of downdrafts. In contrast, for the 2016 case the convection pattern is stronger influenced by the larger mean wind. Here roll convection is found. The updrafts are aligned with the mean wind.

For the 2016 case study, a stronger influence of the entrained air was found in the moisture field. Thus, a connection between the organization of the convection and

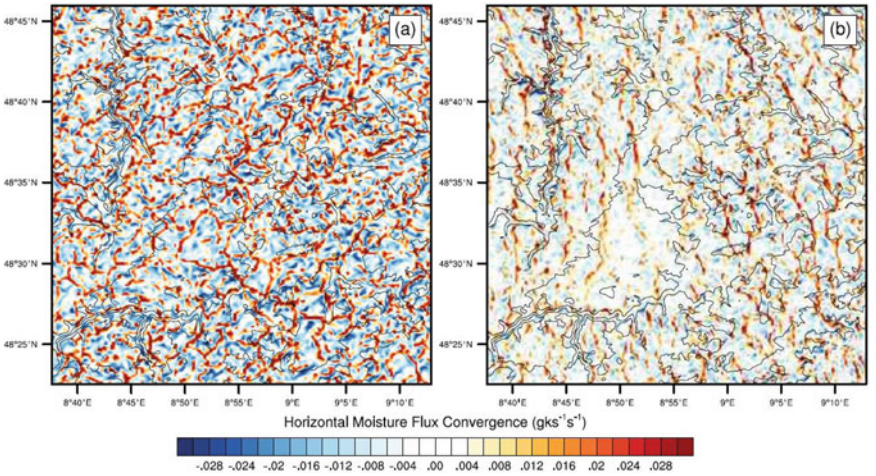

Fig. 19 Instantaneous fields of the horizontal water vapor mixing ratio convergence $[gkg^{-1}s^{-1}]$ for the 2015 case in panel (**a**) and for the 2016 case in panel (**b**). All fields where averaged vertically over the 15 lowermost model levels

the strength of the entrainment can be drawn. For roll convection, the engulfment of entrained air into the PBL seems to be stronger, than for open cell convection.

3 Computational Issues

Table 2 summarizes the applied computer resources for the whole project during the period May 2018 to April 2019, subdivided into the five sub-projects.

Table 2 Core hours used by the different sub-projects between May 2017 and April 2018

Sub-project	Used core-h May 2018 to April 2019
LES-PROC	216776
UAE-1	1004543
UAE-2	474543
VAP-DA	271594
LES-PBL	535607
Total	2503063

References

1. K. Becker, V. Wulfmeyer, T. Berger, J. Gebel, W. Münch, Carbon farming in hot, dry coastal areas: An option for climate change mitigation. Earth Syst. Dyn. **4**, 237–251 (2013)
2. O. Branch, K. Warrach-Sagi, V. Wulfmeyer, S. Cohen, Simulation of semi-arid biomass plantations and irrigation using the WRF-NOAH model—a comparison with observations from Israel. Hydrol. Earth Syst. Sci. **18**, 1761–1783 (2014)
3. V. Wulfmeyer, O. Branch, K. Warrach-Sagi, H.-S. Bauer, T. Schwitalla, K. Becker, The impact of plantations on weather and climate in coastal desert regions. J. Appl. Meteorol. Climatol. **53**, 1143–1169 (2014)
4. V. Wulfmeyer, D.D. Turner, B. Baker, A. Behrendt, T. Bonin, A. Brewer, M. Burban, A. Choukulkar, E. Dumas, R. Hardesty, T. Heus, J. Ingwersen, D. Lange, T. Lee, S. Metzendorf, S. Muppa, T. Meyers, R. Newsom, M. Osman, S. Raasch, A new research approach for obswerving and characterizing land-atmosphere feedback. Bull. Amer. Meteorol. Soc. **99**, 1639–1667 (2018)